Science of the Total Environment 650 (2019) 408–418

Contents lists available at ScienceDirect

Science of the Total Environment

journal homepage: www.elsevier.com/locate/scitotenv

Cu and Co nanoparticles co-doped MIL-101 as a novel adsorbent for efficient removal of tetracycline from aqueous solutions

Jiahui Jin [a,b], Zhaohui Yang [a,b,*], Weiping Xiong [a,b], Yaoyu Zhou [c], Rui Xu [a,b], Yanru Zhang [a,b], Jiao Cao [a,b], Xin Li [a,b], Chengyun Zhou [a,b]

[a] College of Environmental Science and Engineering, Hunan University, Changsha 410082, China
[b] Key Laboratory of Environmental Biology and Pollution Control, Ministry of Education, Hunan University, Changsha 410082, China
[c] College of Resources and Environment, Hunan Agricultural University, Changsha 410128, China

HIGHLIGHTS

- MIL-101 doped with Cu and Co bimetallic nanoparticles was utilized as an adsorbent to remove tetracycline for the first time.
- The synergistic effect between Cu and Co made the adsorption capacity of CuCo/MIL-101 significantly enhanced.
- Electrostatic interaction played an important role in the adsorption process.
- The good reusability and stability of CuCo/MIL-101 proved its potential to remove tetracycline from actual wastewater.

GRAPHICAL ABSTRACT

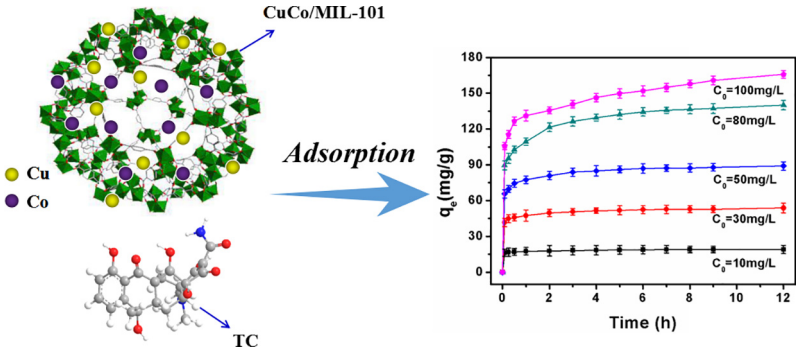

ARTICLE INFO

Article history:
Received 14 June 2018
Received in revised form 12 August 2018
Accepted 31 August 2018
Available online 01 September 2018

Editor: Baoliang Chen

Keywords:
CuCo/MIL-101
Tetracycline
Adsorption
Mechanism

ABSTRACT

Chromium metal-organic framework (MIL-101(Cr)) has been widely studied for removing organic contaminants from aqueous solutions due to its excellent water stability and giant pore size, but its low adsorption capacity limits the application. In this study, a new adsorbent MIL-101 loaded with CuCo bimetallic nanoparticles (CuCo/MIL-101) was successfully fabricated and applied in removal of tetracycline (TC) from aqueous solutions. The adsorption capacity of CuCo/MIL-101 for TC increased by 140% compared with that of pure MIL-101, which may be attributed to the chemical bonding between Cu and Co BNPs in MIL-101 and TC molecules. The effects of pH, ionic strength, humic acid and contact time on the adsorption were also discussed in detail. The results showed that the removal efficiency of TC solution with high concentration (100 mg L^{-1}) by CuCo/MIL-101 was still as high as 82.9%. The data of adsorption kinetics and isotherms could be well fitted by Elovich model and Freundlich model, respectively. According to the fitting parameters, the maximum adsorption capacity of CuCo/MIL-101 reached up to 225.179 mg g^{-1}. Additionally, the adsorption process of TC onto CuCo/MIL-101 was spontaneous and endothermic. Electrostatic interactions could play an important role in the adsorption process. The enhanced adsorption capacity, excellent reusability and water stability demonstrated the potential of CuCo/MIL-101 composite as a novel adsorbent for the removal of TC from aqueous solutions.

© 2018 Elsevier B.V. All rights reserved.

1. Introduction

Antibiotics are extensively used in the prevention and treatment of human and animal diseases, and as growth promoters for livestock,

* Corresponding author at: Hunan University, College of Environmental Science and Engineering, Changsha 410082, China.
E-mail address: yzh@hnu.edu.cn (Z. Yang).

https://doi.org/10.1016/j.scitotenv.2018.08.434
0048-9697/© 2018 Elsevier B.V. All rights reserved.

poultry and fish (Yang et al., 2011; Zhao et al., 2012). Among all antibiotics, tetracycline (TC) ranks second in usage amount in the world due to its broad-spectrum antibacterial activity, accounting for approximately one third of the production and consumption of antibiotics (Wang et al., 2018). However, since TC is difficult to be digested and absorbed by humans and animals, the pollutant is commonly discharged into the environment in its original form through feces or urine, causing serious environmental problems (Priya and Radha, 2014). The residues of TC can be detected in various receiving aquatic environment, even in drinking water (Kemper, 2008; Valcarcel et al., 2011). It was reported that TC concentrations in the sediments of the Yellow River, the Haihe River, the Liaohe River and the Pearl River are over 653 ng g^{-1} (Yang et al., 2010; Zhou et al., 2011). According to Deblonde et al., the concentration of TC in the effluent of the wastewater treatment plant (WWTP) is 2.375 μg L^{-1} (Deblonde et al., 2011). The extensive use and even abuse of TC cause significant risks to human health and the environment. Long-term enrichment of TC in the environment can lead to the microbial resistance to antibiotics and have toxicity to native microorganisms in the aquatic environment (Dantas et al., 2008; Xu et al., 2017). Therefore, it is urgent to remove TC from the environment, especially to minimize the adverse effect on the aquatic ecosystem.

Due to the variable form, low biodegradability, and complex molecular structure of TC, it is difficult to achieve complete removal of TC by conventional methods of wastewater treatment (Seo et al., 2017). Many researchers have employed some physical and chemical treatment methods to remove TC from aqueous solutions, such as adsorption, biodegradation, membrane separation, advanced oxidation, photocatalytic degradation and electrochemical processes (Michael et al., 2013; Wang et al., 2013; Song et al., 2017a; Xiong et al., 2017; Xu et al., 2018; Zhou et al., 2018). Among them, adsorption is superior to other treatment methods since the significant advantages such as simple operation, low cost, low energy requirements and no secondary pollution. Many adsorbents have been investigated for removal of TC from aqueous solutions such as activated carbon (Kim et al., 2010), graphene oxide (Gao et al., 2012), bio-char (Zhou et al., 2017b), clay (Chang et al., 2009), sludge (Ocampo-Pérez et al., 2012), and etc. Nevertheless, their applications are limited due to their relatively low adsorption capacity and poor reusability. Therefore, the development of high-performance and cost-effective adsorbents to remove antibiotics from aqueous solutions is needed.

In recent years, metal-organic frameworks (MOFs), composed of metal ions or clusters and organic linkers, have attracted wide attention due to their special physical and chemical characteristics such as ultra-high surface area, tunable pore size, and easy chemical modifiability (Rowsell and Yaghi, 2004). MOFs have been applied in various fields, such as gas storage and separation, catalysis, sensing and adsorption (Barea et al., 2014). Besides, a great deal of studies have reported on the removal of organic pollutants from aqueous solutions by MOFs (Haque et al., 2010; Hasan et al., 2012; Jiang et al., 2013; Zhu et al., 2015; Xiong et al., 2018a; Xiong et al., 2018b). Due to the large size of TC molecule, a sufficiently large pore size of the adsorbent is the prerequisite to obtain a high adsorption capacity (Hu et al., 2016). However, most of MOFs materials are confined to their microporous structure, and their smaller pore size does not favor the diffusion and mass transfer process of large-sized molecules (Qiu et al., 2008). Among numerous MOFs materials, MIL-101 with mesoporous structure (MIL stands for Material of Institute Lavoisier) is attractive in liquid phase adsorption due to its excellent hydrothermal stability and large pore size. Besides, the coordinated unsaturated Cr^{3+} centers in the framework endow MIL-101 with Lewis acid properties, which contributes to the acid-alkaline interaction between Lewis open metal sites and other basic groups (Hu et al., 2016). Nevertheless, since pure MIL-101 has limited adsorption capacity for contaminants in water, it can be modified by incorporating some active species (such as various acidic or basic functional groups, metal nanoparticles, metal ions, metal oxides, metal salts, etc.) to optimize the performance (Khan et al., 2013). Metal nanoparticles (MNPs) have been widely used due to their higher surface energy, large surface area, small size, and high reactivity. These properties provide rapid adsorption rates and high adsorption capacity for eliminating pollutants in water. Transition metals such as Cu, Fe, Co and Ni have a slightly lower reactivity than noble metals (such as Au, Ag, Pd), but their low cost and wide availability make them alternatives for noble metals. Bimetallic nanoparticles (BNPs) exhibit remarkably enhanced physical and chemical properties over the monometallic NPs due to the synergistic effect between the two metals, and are widely used in various fields (Jiang and Xu, 2011). Incorporating BNPs into MOFs has been extensively used for synergistic catalysis, which seems to be an encouraging method of the modification for enhancing the adsorption performance in liquid phase (Chen et al., 2015; Qu et al., 2017). Therefore, it is considered to load CuCo BNPs on the MIL-101 to enhance the performance and availability of MIL-101. To our knowledge, currently there is no report about the removal of TC from aqueous solutions by CuCo/MIL-101 composite.

The focus of this study is to synthesize CuCo/MIL-101 composite and apply it to remove TC from aqueous solutions. The physical and chemical properties of prepared samples were characterized by various characterization methods including XRD, SEM, TEM, EDS, BET, FT-IR, TGA, XPS, zeta potential and particle size. The adsorption behavior of TC onto CuCo/MIL-101 was investigated systematically through batch adsorption experiments. Adsorption kinetics, isotherms and thermodynamics were also explored in detail. Meanwhile, the effects of pH, ionic strength, humic acid and contact time on TC adsorption were examined. Finally, the reusability of adsorbent was evaluated by recycle experiments.

2. Materials and methods

2.1. Chemicals

Chromium nitrate nonahydrate ($Cr(NO_3)_3 \cdot 9H_2O$, 99%) was obtained from Xilong Chemical Co., Ltd. (Guangdong, China). *N*,*N*-dimethylformamide (DMF, 99.5%), 1,4-benzenedicarboxylic acid (H_2BDC, 99%), hydrofluoric acid (HF, 40%), ammonium fluoride (NH_4F, >96%), sodium borohydride ($NaBH_4$, >98%), copper nitrate trihydrate ($Cu(NO_3)_2 \cdot 3H_2O$, >99%), cobalt chloride hexahydrate ($CoCl_2 \cdot 6H_2O$, >99%) were purchased from Sinopharm Chemical Regent Co., Ltd. (Shanghai, China). Tetracycline hydrochloride ($C_{22}H_{24}N_2O_8 \cdot HCl$) was supplied by Bomei biotechnology Co., Ltd. (Hefei, China). All the reagents and solvents were in analytical grade and used without further purification. Ultrapure water (resistivity of 18.25 MΩ cm^{-1}) was used to prepare stock solutions and other solutions throughout the experiment.

2.2. Preparation of adsorbents

2.2.1. Synthesis of MIL-101

MIL-101 was prepared by a hydrothermal method according to the previous literature with some modifications (G. Férey et al., 2005). Typically, 4.2 g $Cr(NO_3)_3 \cdot 9H_2O$, 1.661 g H_2BDC, and 0.5 mL HF were added to 70 mL of water. The mixture was stirred for 15 min, then poured into a 100 mL Teflon-lined stainless steel autoclave and heated at 220 °C for 8 h. After being naturally cooled to room temperature, the resulting dark green mixture was filtered using a sand core funnel (G2) to remove unreacted terephthalic acid. The MIL-101 was purified as following steps. Firstly, the resulting material by centrifugation was washed three times with ethanol and DMF solutions, respectively. Secondly, the green solid was soaked in NH_4F solution and heated at 70 °C for 24 h in a thermostatic water bath. Finally, the obtained product was dried at 150 °C for 12 h under vacuum.

2.2.2. Preparation of Cu/MIL-101, Co/MIL-101 and CuCo/MIL-101

The Cu/MIL-101, Co/MIL-101 and CuCo/MIL-101 were obtained by following a previously reported approach (Li et al., 2015). Generally, 100 mg of MIL-101 was suspended in 20 mL of anhydrous n-hexane and homogenized by sonication for 20 min. After stirring for 2 h, 0.15 mL of the desired concentration of $Cu(NO_3)_2 \cdot 3H_2O$ or/and $CoCl_2 \cdot 6H_2O$ solution was added dropwise within 15 min with vigorous stirring. Subsequently, the obtained solution was further stirred for 1 h. The solid deposited on the bottom was dried under vacuum. The molar amounts of $(Cu^{2+} + Co^{2+})$ was 0.034 mmol relative to the addition of 100 mg of MIL-101, and the different molar ratio of Cu^{2+} : $(Cu^{2+} + Co^{2+})$ was 0, 0.1, 0.2, 0.3, 0.4, 0.5, 0.6, 0.7, 0.8, 0.9 and 1.0, respectively. The freshly prepared $NaBH_4$ solution was added into the obtained Cu^{2+}/MIL-101, Co^{2+}/MIL-101 and $Cu^{2+}Co^{2+}$/MIL-101 while maintaining vigorous stirring. The resulting products were filtered and washed with water several times and finally dried at 60 °C for 12 h under vacuum. The obtained adsorbents were sequentially named Co/MIL-101, MLB-1, MLB-2, MLB-3, MLB-4, MLB-5, MLB-6, MLB-7, MLB-8, MLB-9 and Cu/MIL-101 according to above mentioned ration of Cu^{2+} : $(Cu^{2+} + Co^{2+})$.

2.3. Characterization

The crystalline structure of synthesized samples was characterized by X-ray powder diffraction (XRD, D/Max-2500, Rigaku, Japan) with a scan speed of 5° min^{-1} in the range from 3 to 80°. The morphological structure of the materials was obtained by field emission scanning electron microscopy (FE-SEM, FEI Quanta 400, USA) and transmission electron microscope (TEM, FEI G2 F20). Energy dispersive X-ray spectroscopy (EDS) was performed coupled with TEM. The Brunauer-Emmett-Teller (BET) surface area, pore volume and pore size of samples were measured by means of nitrogen adsorption-desorption (Quantachrome, USA). The Fourier transform infrared spectrum was obtained by a Nicolet 5700 Spectrometer in KBr pellet at room temperature (Nicolet, USA). To analyze the thermal stability of the samples, a thermal weight loss curve from room temperature to 800 °C (TGA, Q500, USA) was measured. The chemical state of elements was determined by X-ray photoelectron spectroscopy (XPS, Thermo Fisher Scientific-ESCALAB 250Xi, USA). The zeta potentials and the particle sizes of adsorbents were measured by a Zeta-sizer Nano-ZS (Malvern, UK).

2.4. Adsorption experiments

A standard stock solution of 1000 mg L^{-1} TC was prepared and stored in the refrigerator at 4 °C. All other experimental concentrations of TC solutions were obtained by diluting the stock solution. 50 mg of adsorbent was added to a 250 mL conical flask containing 100 mL of the desired TC solution. The conical flasks were placed in a thermostatic water bath oscillator with shaking speed of 150 rpm at 298 K for batch adsorption experiments. Samples were taken at given time intervals, centrifuged at 5000 rpm for 10 min, and filtered by using 0.45 μm PVDF disposable filters. Then, the concentration of TC was measured by a UV–vis spectrophotometer at 357 nm (UV-2700, SHIMADZU, Japan).

TC solution of 50 mg L^{-1} was chosen to investigate the influences of pH, ionic strength and humic acid on the adsorption. The TC solutions with different pH value (range from 3 to 11) were obtained by adding 0.1 M HCl or NaOH with a pH meter (FE20, China). NaCl and Na_2SO_4 with different concentrations (0.02, 0.04, 0.06, 0.08, and 0.1 M) were selected as metal salts to analyze the impact of ionic strength on adsorption. The influence of humic acid concentration (0, 5, 10, 15 and 20 mg L^{-1}) was also examined. Different concentrations of TC solutions (10, 30, 50, 80 and 100 mg L^{-1}) were used for exploring the adsorption kinetics. When the isotherm adsorption and adsorption thermodynamics were studied, a series of TC solutions with different concentrations were adequately reacted at different temperatures (298, 308 and 318 K) for 24 h. Detailed information on the kinetic models and isotherms models involved in this study and the equations for various calculations were given in Table S1.

2.5. Recycle experiments

Reusability of the adsorbent is directly related to its commercial application. Therefore, recycle experiments were performed to evaluate the regenerability and reusability of the adsorbent. For this purpose, the used adsorbent was first soaked in ethanol solution and sonicated for 2 h to reach completely desorption condition. Then, the regenerated adsorbent was filtered, washed with water, dried and used for the next adsorption experiment.

3. Results and discussion

3.1. Characterization of the prepared samples

As shown in Fig. 1, all of the diffraction peaks of the synthesized MIL-101 matched well with the simulated XRD pattern of MIL-101 (G. Férey et al., 2005), indicating that MIL-101 was successfully synthesized. The intensities of these characteristic peaks were high, and no other phases or impurity peaks were observed, which indicated that the prepared samples had a higher degree of crystallinity. The XRD patterns of the Cu/MIL-101, Co/MIL-101 and CuCo/MIL-101 showed no noticeable differences compared with pure MIL-101, suggesting that the structure of MIL-101 was not destroyed and its main framework still kept intact. In addition, no diffraction peak of the MNPs in XRD was observed, possibly because the size of MNPs was extremely small, which proved that the synthesized copper or cobalt was at zero price.

SEM images (Fig. 2a–d) revealed that the typical octahedral crystal morphology of MIL-101 remained unchanged after the addition of Cu or/and Co nanoparticles. From the TEM images of MLB-8 in Fig. 2e–f, the obvious black spots can be easily identified in the light gray regions of MLI-101. As can be seen from the EDS elemental mapping analysis of MLB-8 in Fig. 3e–f, the purple and blue dots representing the Cu element and Co element, respectively, were uniformly distributed on the surface of MLB-8. For comparison, the mappings of C, O and Cr elements were also depicted in Fig. 3b–d. Combining the analysis of TEM and EDS mapping, it was confirmed that part of CuCo BNPs were successfully doped into the pores of MIL-101, and some of the nanoparticles were accumulated on the surface of MIL-101. EDS analysis further confirmed the presence of Cu and Co elements in MIL-101 (Fig. S1).

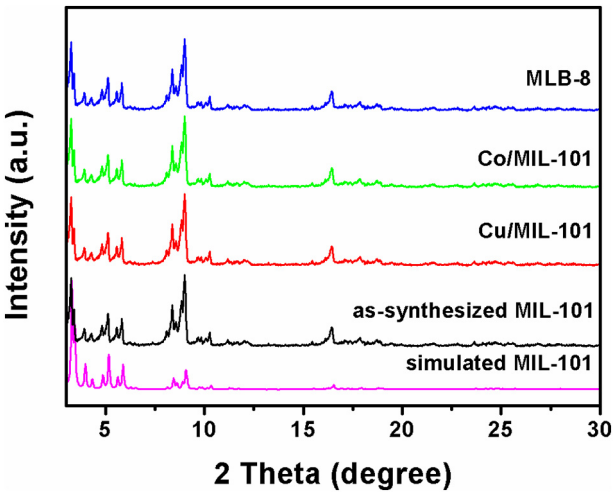

Fig. 1. The XRD patterns of pure MIL-101 and MNPs/MIL-101.

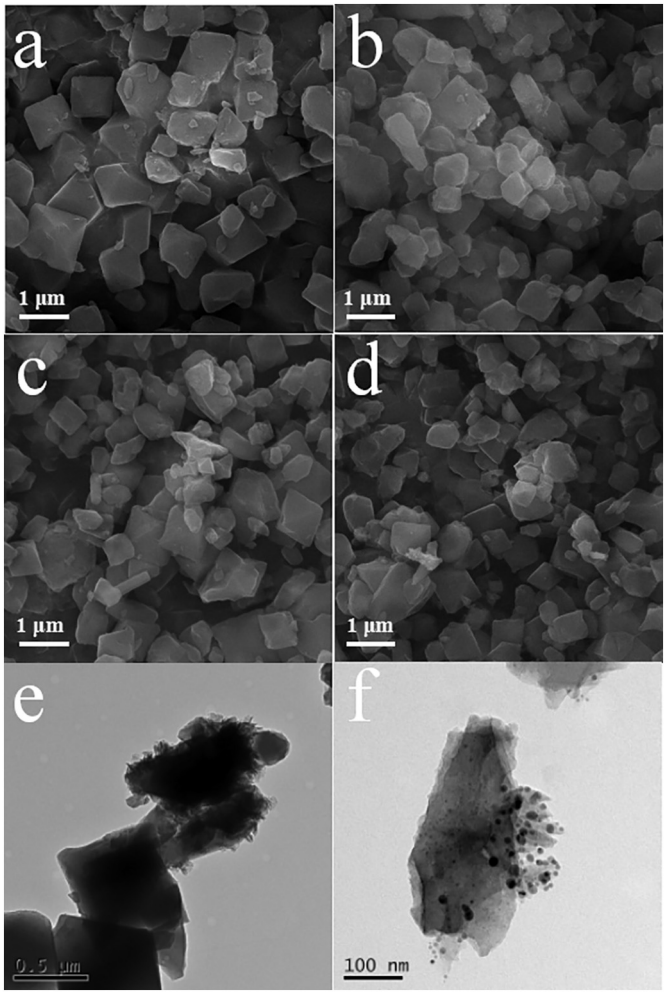

Fig. 2. The SEM images of MIL-101(Cr) (a), Cu/MIL-101 (b), Co/MIL-101 (c) MLB-8 (d), and TEM images of MLB-8 (e–f).

The particle sizes of different adsorbents were analyzed by Zetasizer Nano-ZS (Malvern, UK). The particle size of MIL-101 was 804.2 nm, which was consistent with the previous report, implying the material was well-synthesized (Hu et al., 2013). After modification, the particle sizes of Cu/MIL-101, Co/MIL-101 and MLB-8 were 1088.0, 989.2 and 998.4 nm, respectively.

The nitrogen adsorption-desorption isotherms and summarized textural properties were shown in Fig. 4a and Table 1. Both MIL-101 and MNPs/MIL-101 exhibited type I isotherm, revealing the presence of micropores in these four materials. The surface area of MIL-101 was 3323.3 $m^2\ g^{-1}$, while that of Cu/MIL-101, Co/MIL-101 and MLB-8 decreased to 2342.6, 2787.6 and 2422.7 $m^2\ g^{-1}$, respectively. The reduction in BET specific surface area and total pore volume may be attributed to the blocking of cavities or pores caused by the fact that MNPs occupied part of cavities of the MIL-101, indicated that the metal nanoparticles were successfully introduced into the MIL-101 (Qi et al., 2018).

The FT-IR spectroscopy of MIL-101, Cu/MIL-101, Co/MIL-101 and CuCo/MIL-101 were presented in Fig. 4b. These four materials showed similar spectra because of the extremely low MNPs content. It was obvious that the ν_{as} (COO) and ν_s (COO) in the MIL-101 were located at 1539 and 1401 cm^{-1}, respectively (Maksimchuk et al., 2008). The weak and narrow bands at 749 and 1017 cm^{-1} were displayed to correspond to γ (CH) and δ (CH) vibrations of the aromatic rings, respectively. Weak bands within the spectral range of 700–400 cm^{-1} could be attributed to in-plane and out-of-plane bending modes of COO-groups. It proved that the structure of MIL-101 kept intact after loading MNPs, which was in accordance with the results of XRD measurements.

The thermal stability of MIL-101 and MLB-8 were measured by the TGA analysis curves (Fig. S2). Two weight loss steps in the range of 20–100 °C and 300–500 °C could be observed in both MIL-101 and MLB-8. The initial weight loss could be assigned to the loss of guest water molecules. The sharp decrease in the weight of the second step may be due to the removal of OH/F groups and the collapse of the MIL-101 framework (G. Férey et al., 2005). Although the thermal stability of MIL-101 decreased slightly after doped into CuCo BNPs, its main framework remained stable up to 300 °C.

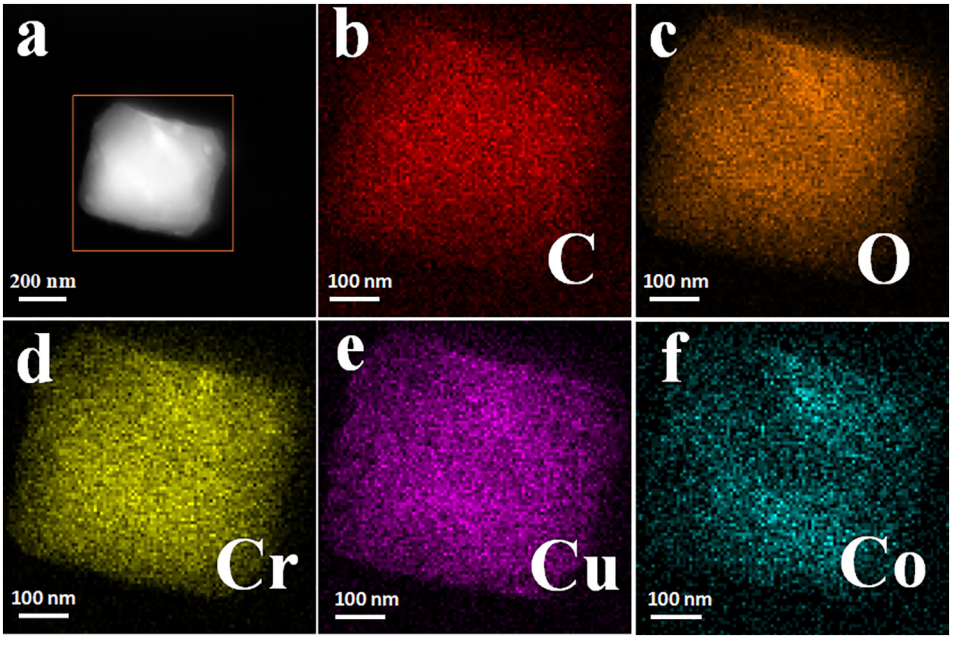

Fig. 3. TEM mapping of partially selected element of MLB-8: C (b), O (c), Cr (d), Cu (e) and Co (f).

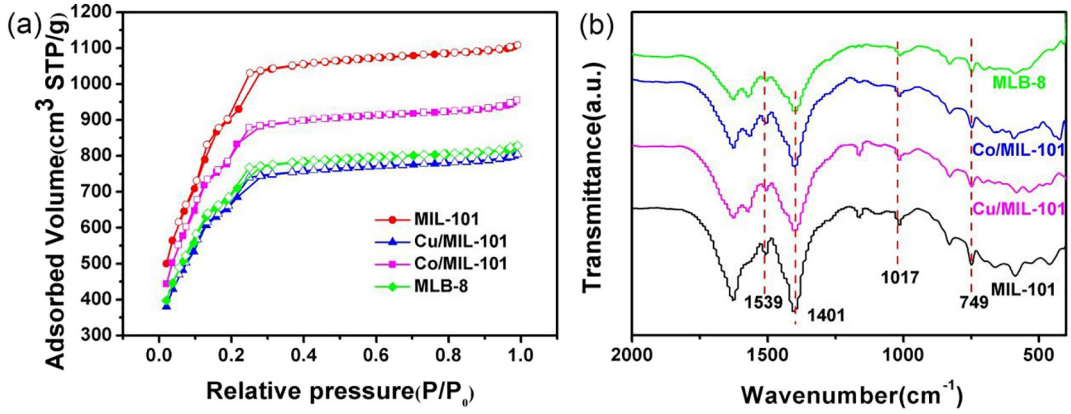

Fig. 4. N_2 adsorption-desorption isotherms (a) and FT-IR spectra (b) of MIL-101, Cu/MIL-101, Co/MIL-101 and MLB-8.

The surface elemental composition and valence state in the Cu/MIL-101, Co/MIL-101 and CuCo/MIL-101 were determined by X-ray photoelectron spectroscopy (XPS) measurement (Fig. 5). The XPS survey spectrum in Fig. 5a presented the presence of five elements of C, O, Cr, Cu and Co in the CuCo/MIL-101 sample, which was consistent with the previous analysis of EDS. Before Ar etching, the binding energies of Co in Co/MIL-101 and CuCo/MIL-101 corresponded to that of CoO due to oxidation of materials in the air, which was similar to the previous literature (Li et al., 2015). After 10 min of Ar etching, both Cu and Co were observed to be in the reduced state. The peaks at 932.6 and 952.4 eV corresponded to Cu (0) $2p_{3/2}$ and Cu (0) $2p_{1/2}$, while 777.9 and 793.0 eV were attributed to the Co (0) $2p_{3/2}$ and Co (0) $2p_{1/2}$. This further proved the fact that MNPs, rather than metal oxides, were loaded on the MIL-101 framework.

3.2. The effect of Cu^{2+}: (Cu^{2+} + Co^{2+}) and solution pH

The results of TC adsorption by different samples were depicted in Fig. S3. Obviously, the adsorption capacity of pure MIL-101 was only 24.8 mg g^{-1}. All MNPs/MIL-101 samples had a better adsorption performance than the pure MIL-101. This may be due to the strong affinity between MNPs and TC molecules. The adsorption capacity of CuCo/MIL-101 for TC firstly raised with the increase of Cu^{2+}: (Cu^{2+} + Co^{2+}) ratio and then decreased gradually. When the ratio was 0.8, the adsorption capacity reached the highest value of 83.8 mg g^{-1}. The adsorption performance of samples followed the order of MIL-101 < Co/MIL-101 < Cu/MIL-101 < MLB-8, indicating there was a synergistic effect between Cu and Co nanoparticles supported in MIL-101. Additionally, the adsorption capacity of Cu/MIL-101 was remarkably higher than that of Co/MIL-101, which may be attributed to the geometric effects in the electron effects (Ferrando et al., 2008). It was also possible that Co nanoparticles were not stable in solution or air due to agglomeration and oxidation caused by magnetism, as evidenced by previous XPS analysis results. In this study, although the specific surface area of MLB-8 decreased by 900.6 m^2 g^{-1} compared to MIL-101, the adsorption capacity increased about 2.4 times. After introduction of CuCo BNPs, in addition to physical adsorption between MLB-8 and TC, there may be a strong chemical interaction, which greatly promoted the adsorption efficiency of TC.

Table 1
The parameters of the porous structure for different adsorbents.

Adsorbents	BET surface area (m^2 g^{-1})	Pore volume (cm^3 g^{-1})
MIL-101	3323.271 ± 205.710	1.716 ± 0.106
Cu/MIL-101	2342.648 ± 140.559	1.244 ± 0.075
Co/MIL-101	2787.593 ± 189.85	1.477 ± 0.101
MLB-8	2422.685 ± 157.475	1.282 ± 0.083

Moreover, the solution pH has a significant impact on adsorption. Variation of solution pH could change the protonation state of functional groups on the adsorbent and composition of TC molecule. As revealed in Fig. 6a, TC is a typical amphoteric molecule. The three dissociation constants in solution determined that the composition of TC mainly including cation (TC^+) (pH < 3.3), molecule (TC^0) (3.3 < pH < 7.7), anions (TC^-) (7.7 < pH < 9.7) and (TC^{2-}) (pH > 9.7) (Zhao et al., 2012; Duan et al., 2014). Fig. 6b showed the effect of solution pH value on TC adsorption. It was clear that the adsorption of TC onto MLB-8 was strongly related to the solution pH value. The optimal adsorption capacity of MLB-8 for TC was observed when pH was 9.0 and the removal efficiency was as high as 86%, indicating that TC had a higher affinity with the surface of MLB-8 at pH 9.0. The adsorption capacity gradually decreased when pH value was less than or greater than 9.0. Especially, the amount of adsorption reduced sharply when the pH value was <4.0, and the removal rate was only 27% when pH value was 3.0. It was certain that the surface charge of the adsorbent played an important role during the adsorption process. The zero potential point (pH_{ZPC}) of MLB-8 was approximately 9.3 (Fig. S4). Obviously, the surface of MLB-8 was positively charged when the solution pH < pH_{ZPC}. There existed electrostatic repulsive force between the positively charged MLB-8 and cationic form of TC at pH 3.0, which resulted in poor adsorption. When pH value was increased from 4.0 to 7.7, TC was predominantly presented in zwitterionic form, rendering them almost non-electrostatic attractive or repulsive interaction with MLB-8. And their removal efficiency was significantly improved compared to that of at pH 3.0, suggesting that there existed non-electrostatic interactions between adsorbent and TC, such as π-π stacking and hydrogen bonding forces. When 7.7 < pH < pH_{ZPC}, the excellent adsorption performance could be explained by the dominant electrostatic attraction between the positively charged MLB-8 and anionic form of TC. However, when pH > pH_{ZPC}, the decrease of adsorption efficiency was due to the enhanced repulsive force between the negatively charged MLB-8 and anionic form of TC.

3.3. The effect of ionic strength and humic acid

The influence of ionic strength on TC removal was shown in Fig. 7a. On the one hand, the general trend was similar whether NaCl or Na_2SO_4 was added into solution, and the adsorption capacity decreased with the ionic strength increased. This phenomenon may be due to the electrostatic shielding effect caused by the addition of NaCl or Na_2SO_4, thereby inhibiting the electrostatic interaction between the anionic form of TC and positively charged MLB-8 (Gao et al., 2012). It was also possible that Cl^- or SO_4^{2-} could combine with the active sites on the MLB-8, and the competition with TC reduced the amount of TC adsorbed onto the MLB-8 (Yu et al., 2014). On the other hand, the inhibition effect of Na_2SO_4 on the TC adsorption was greater than that of NaCl, and the

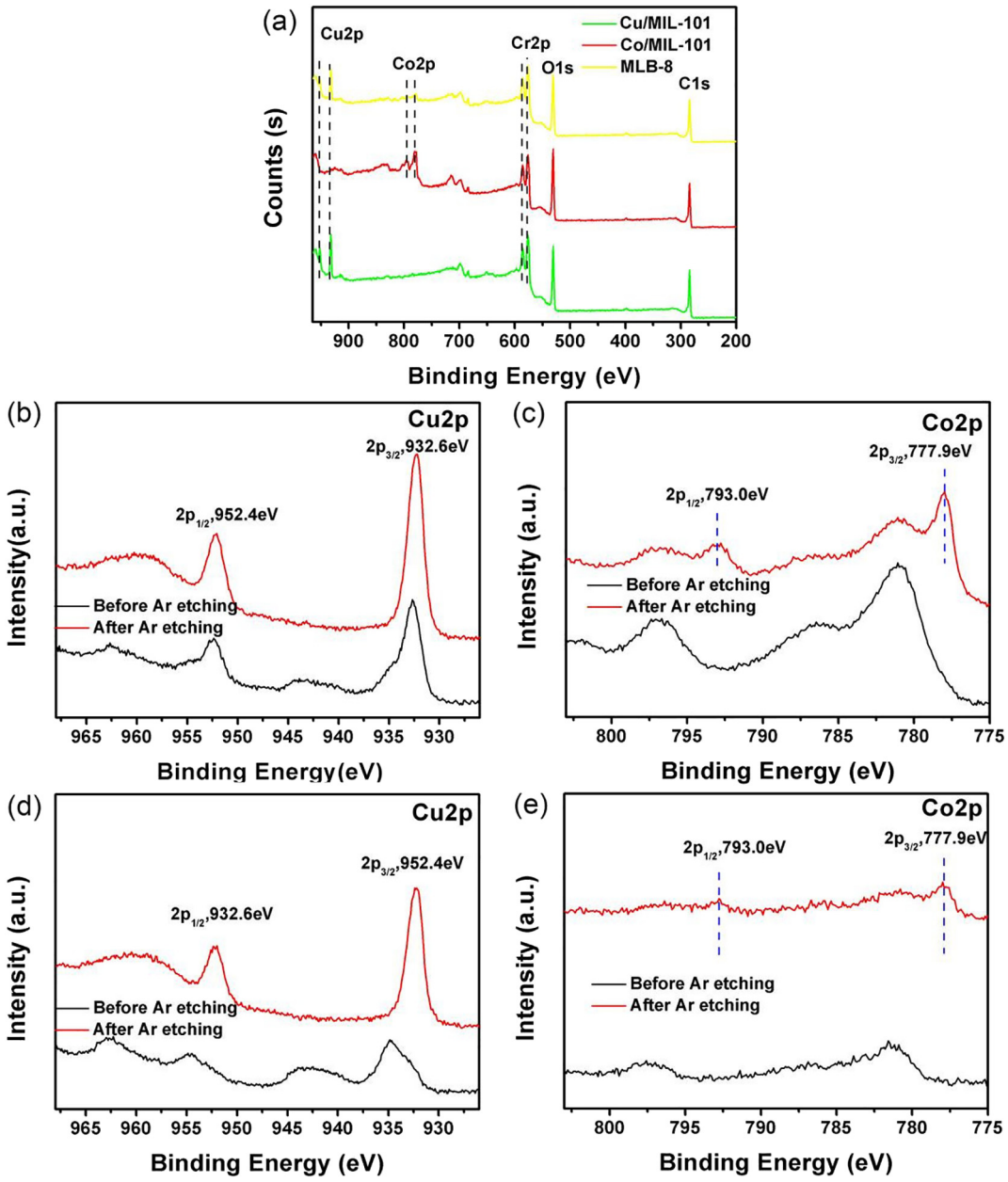

Fig. 5. The XPS spectra of Cu/MIL-101, Co/MIL-101 and MLB-8: survey scan (a), Cu/MIL-101 (b), Co/MIL-101 (c), and MLB-8 (d, e) before and after Ar etching.

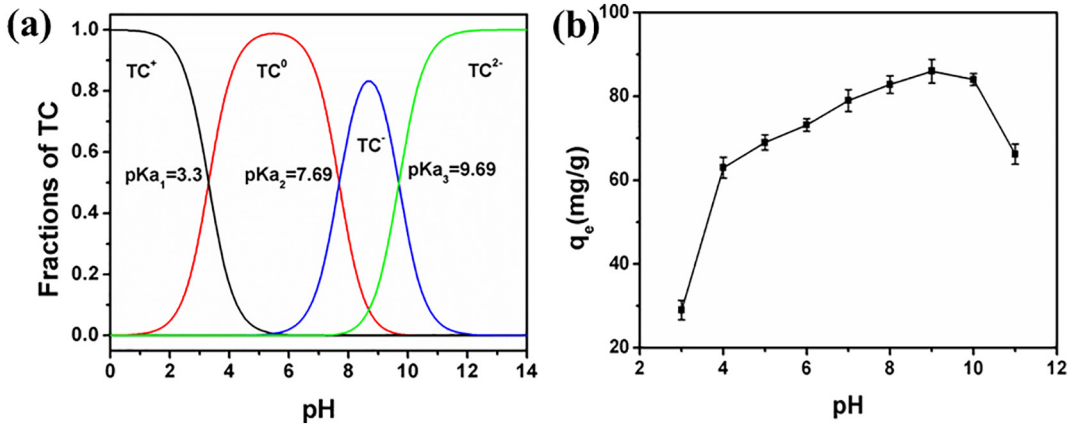

Fig. 6. TC species at different pH (a); Effect of solution pH on the adsorption of TC onto MLB-8 (b). Reaction conditions: C_0 (TC) = 50 mg L^{-1}, m/V = 0.5 g L^{-1}, T = 298 K.

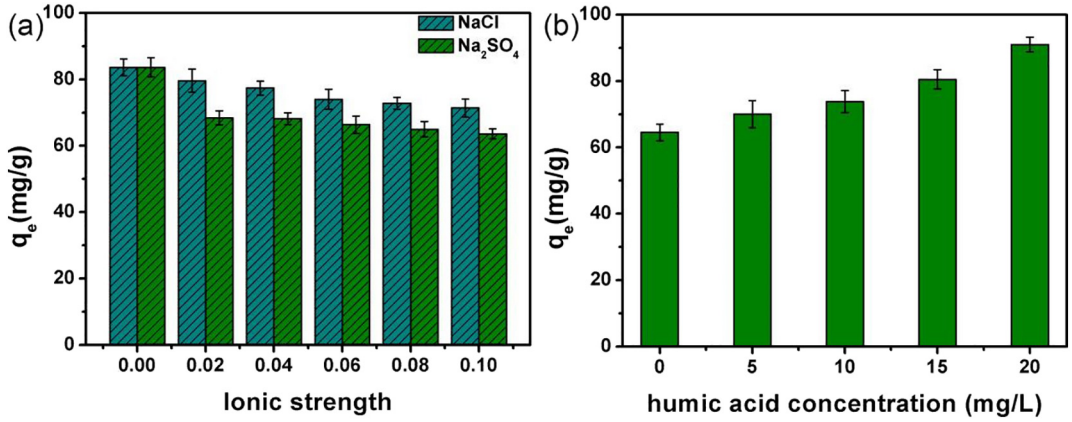

Fig. 7. Effects of ionic strength (a) (reaction conditions: C_0 (TC) = 50 mg L^{-1}, m/V = 0.5 g L^{-1}, pH = 9, T = 298 K.) and humic acid (b) (reaction conditions: C_0 (TC) = 50 mg L^{-1}, m/V = 0.5 g L^{-1}, pH = 4.8, T = 298 K.) on the adsorption of TC onto MLB-8.

removal efficiency decreased from 83.6% to 63.6% and 71.4% (ionic strength from 0 to 0.1 mol L^{-1}), respectively. This could be explained by the fact that SO_4^{2-} had more negative charges than Cl^- at the same concentration, thus causing a stronger competitive adsorption with TC.

Humic acid, mainly derived from microbial degradation of dead plants, is widely distributed in natural water. It contains many functional groups and can interact with other substances through strong π-π stacking (Pils and Laird, 2007; Yang et al., 2017). As shown in Fig. 7b, the presence of humic acid remarkably promoted the adsorption of TC, which may be ascribed to complicated surface complexation in the MLB-8-HA-TC ternary system. HA was found to have a negative zeta potential at pH > 1.5, probably due to the dissociation of carboxyl (—COOH) (Yan and Bai, 2005). At pH 4.8, TC molecule existed in the form of TC^+ and TC^0, which can combine with deprotonated sites (mainly —COOH) on HA. At the same time, the negatively charged HA could interact with positively charged MLB-8 through electrostatic attraction. It suggested that HA might act as a bridge to connect the surface of MLB-8 with TC molecules (Gu et al., 1994; Zhao et al., 2011).

3.4. Adsorption kinetics

The influence of contact time on the TC adsorption at different initial concentrations was presented in Fig. 8. After 12 h of adsorption, the removal percentages were 95.8%, 89.7%, 89%, 87.5% and 82.9% with initial TC concentrations of 10, 30, 50, 80 and 100 mg L^{-1}, respectively. Obviously, adsorption was divided into two stages. Initially, the TC adsorption onto the MLB-8 was particularly rapid, and then gradually slowed down over time until equilibrium was achieved. Furthermore, TC molecules were almost completely adsorbed within 60 min for initial TC concentration of 10 mg L^{-1}, whereas the time to attain equilibrium was longer at higher TC concentrations. In the first 5 min, a significant increase of TC uptake was mainly due to the presence of a great quantity of vacant adsorption sites on the adsorbent. Subsequently, the amount of adsorption decreased since the adsorption sites reached saturated or remaining sites were less attractive to TC molecules (Wang et al., 2016).

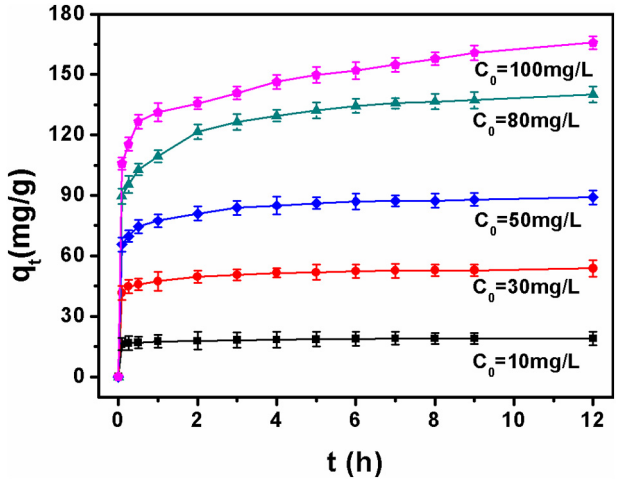

Fig. 8. Effect of contact time on the adsorption of TC. Reaction conditions: C_0 (TC) = 10, 30, 50, 80 and 100 mg L^{-1}, m/V = 0.5 g L^{-1}, pH = 9.0, T = 298 K.

Kinetics studies are important to determine the rate of adsorption process and provide some valuable information for subsequent mechanism analysis. Therefore, several typical kinetics models, pseudo-first-order, pseudo-second-order and Elovich models were exploited to understand the adsorption dynamics of TC onto MLB-8. The adsorption kinetics model parameters have been determined by the average relative error (ARE), and the equation was shown in as follow (Zhou et al., 2017a):

$$ARE = \sum_{i=1}^{n} \left| \frac{q_{e,\,\exp} - q_{e,cal}}{q_{e,\,\exp}} \right| \quad (1)$$

where "*exp*" and "*cal*" presented the experimental and calculated values, respectively.

The parameters obtained from non-linearized forms of the kinetic equations can be seen in Table S2 and the experimental and theoretical data were presented in Fig. S5. The results showed that the Elovich model was best fitted with the experimental data, because it presented the highest values of determination coefficients R^2 (0.985–0.996) and lowest values of average relative error ARE (0.043–0.300). It suggested that the adsorption of TC onto MLB-8 was mainly dominated by the chemisorption involving chemical bonding and electrostatic interactions, which will be discussed in detail in the analysis of adsorption mechanism. As an empirical formula, the Elovich model assumed that the solid surface was energetically heterogeneous, and the desorption and interactions between the adsorbed species do not affect the kinetics of adsorption at low surface coverage. Additionally, the parameters, α (g mg^{-1} min^{-2}) and β (mg g^{-1} min^{-1}), represented the initial adsorption rate and desorption constant, respectively (Pezoti et al., 2016; Li et al., 2017; Ronix et al., 2017). As can be seen from Table S2, the values of α (ranged from 4.430E+3 to 8.074E+14) for three TC concentrations were much higher than β values (ranger from 0.089 to 0.793), indicating an effective adsorption interaction between MLB-8 and TC. Furthermore, the value of α became smaller (lower initial

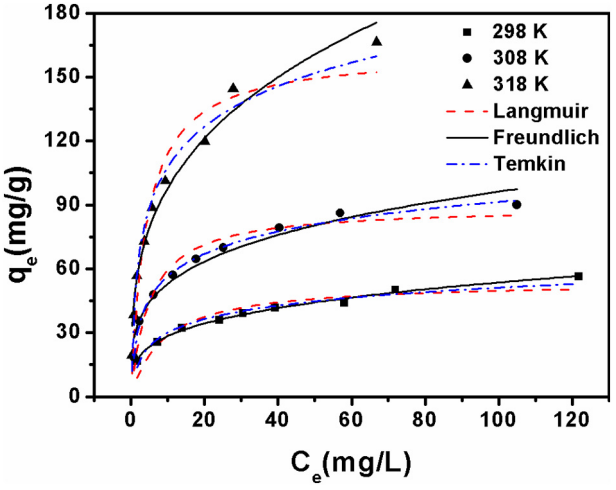

Fig. 9. The isotherm models for adsorption of TC onto MLB-8. Reaction conditions: m/V = 0.5 g L^{-1}, pH = 4.8, t = 24 h, T = 298, 308 and 318 K.

adsorption rate) with the increase of concentration, indicating that the interaction between adsorbent and adsorbate was weakened.

3.5. Adsorption isotherms

The adsorption isotherms can reveal how the adsorbed TC molecules distribute between the solid and liquid phases when the adsorption equilibrium is reached (Xie et al., 2016). Three adsorption isotherm models, Langmuir, Freundlich and Temkin were adopted to fit the experiment data. The model parameters for the three isotherms have also been determined by the average relative error (ARE) using the iterative method. The fitting results were performed in Fig. 9, the relevant parameters were listed in Table 2.

It was obvious that comparing with the Langmuir model and Temkin model, the Freundlich model fitted the experimental data better because it had higher determination coefficients (R^2). Besides, the Freundlich model showed lower values of average relative error (ARE). For Freundlich model, it suggested that TC was a multi-layered adsorption on the heterogeneous surface of MLB-8. The results further demonstrated that physical interaction might play a crucial role during the adsorption process. The value of heterogeneity factor 1/n, which represents the bond distribution, is usually between 0 and 1. The smaller 1/n is, the more favorable adsorption will be (Song et al., 2017b). The 1/n of this experiment ranged from 0.259 to 0.308, far <2, which favored the adsorption of TC. Besides, the maximum equilibrium adsorption capacity of TC by MLB-8 enhanced with the increase of temperature and was 59.968, 106.840 and 225.179 mg g^{-1} at 298, 308 and 318 K, respectively, which was remarkably higher than many adsorbents (Table S3). This phenomenon revealed the process of TC adsorption onto MLB-8 was endothermic.

3.6. Thermodynamics studies

Adsorption thermodynamics could provide depth information about the change of the inherent energy and help to understand the impact of temperature on the adsorption process. Therefore, the adsorption behaviors of different concentrations of TC were investigated at 298, 308 and 318 K, respectively. Thermodynamic parameters including standard Gibbs free energy (ΔG°), standard enthalpy change (ΔH°), and standard entropy change (ΔS°) are calculated according to the following equations (Liu and Xu, 2007; Liu and Liu, 2008; Liu, 2009):

$$\Delta G^\circ = -RT \ln K_a \quad (2)$$

$$K_a = 10^6 K_L \quad (3)$$

$$\ln K_a = \frac{\Delta S^\circ}{R} - \frac{\Delta H^\circ}{RT} \quad (4)$$

where R is the gas constant (8.314 J mol^{-1} K^{-1}), T is the absolute temperature (K). K_a is the thermodynamic equilibrium constant without units, which can be obtained by multiplying Langmuir equilibrium constant K_L (L mg^{-1}) by 10^6 (Milonjic, 2007; Milonjic, 2009). The slope and intercept of the plot of ln K_a versus $1/T$ are $-\Delta H^\circ/R$ and $\Delta S^\circ/R$, respectively.

The thermodynamics results were given in Table 3. The values of ΔG° at all experimental temperatures were negative, proving that the adsorption of TC onto MLB-8 was spontaneous and thermodynamically favorable. Furthermore, ΔG° value decreased from −28.805 to −32.731 kJ mol^{-1} when the temperature increased from 298 to 318 K, which confirmed that the adsorption reaction was more favorable at a relatively higher temperature. The obtained value of ΔH° was 29.851 kJ mol^{-1}, which may be attributed to the adsorption of TC onto MLB-8 was a physico-chemical adsorption process rather than a pure physisorption or chemisorption process (Kara et al., 2003; Oepen et al., 1991). The positive value of ΔH° revealed the typical endothermic nature of the adsorption process, which was consistent with the results of adsorption isotherms. The positive value of ΔS° manifested that an increased randomness at the adsorbent-adsorbate interface. In conclusion, raising the temperature as far as possible would be beneficial to TC adsorption on the MLB-8.

Table 3
Thermodynamic parameters for adsorption of TC onto MLB-8.

T (K)	lnK_a	ΔG° (kJ mol^{-1})	ΔH° (kJ mol^{-1})	ΔS° (kJ K^{-1} mol^{-1})
298	11.626	−28.804		
308	12.201	−31.243	29.851	0.197
318	12.380	−32.731		

3.7. Regenerability analysis

The regenerability of adsorbent is also an important parameter for evaluating the adsorption performance, which is of great significance for practical applications. The adsorption performance of reusable MLB-8 was depicted in Fig. S6(a). Although the adsorption of TC decreased slightly with the increase of cycle numbers, MLB-8 still maintained a high adsorption capacity for TC after reusing four times. Most of MOFs have poor water stability, which greatly limits their practical application in liquid phase adsorption. Therefore, this research also investigated the stability of MLB-8 in aqueous solutions. As revealed in

Table 2
Adsorption isotherm parameters of TC onto MLB-8 at different solution temperature.

T (K)	Langmuir				Freundlich					Temkin			
	K_L (L mg^{-1})	q_m (mg g^{-1})	R^2	ARE	Q_m (mg g^{-1})	K_F (L mg^{-1})	1/n	R^2	ARE	K_T (L mg^{-1})	f	R^2	ARE
298	0.112	54.040	0.867	0.985	59.968	14.985	0.277	0.992	0.199	9.179	2.629	0.964	0.508
308	0.199	89.125	0.949	0.905	106.840	29.221	0.259	0.994	0.203	15.146	4.169	0.955	0.816
318	0.238	161.858	0.943	1.400	225.179	48.222	0.308	0.981	0.783	27.345	5.143	0.970	1.167

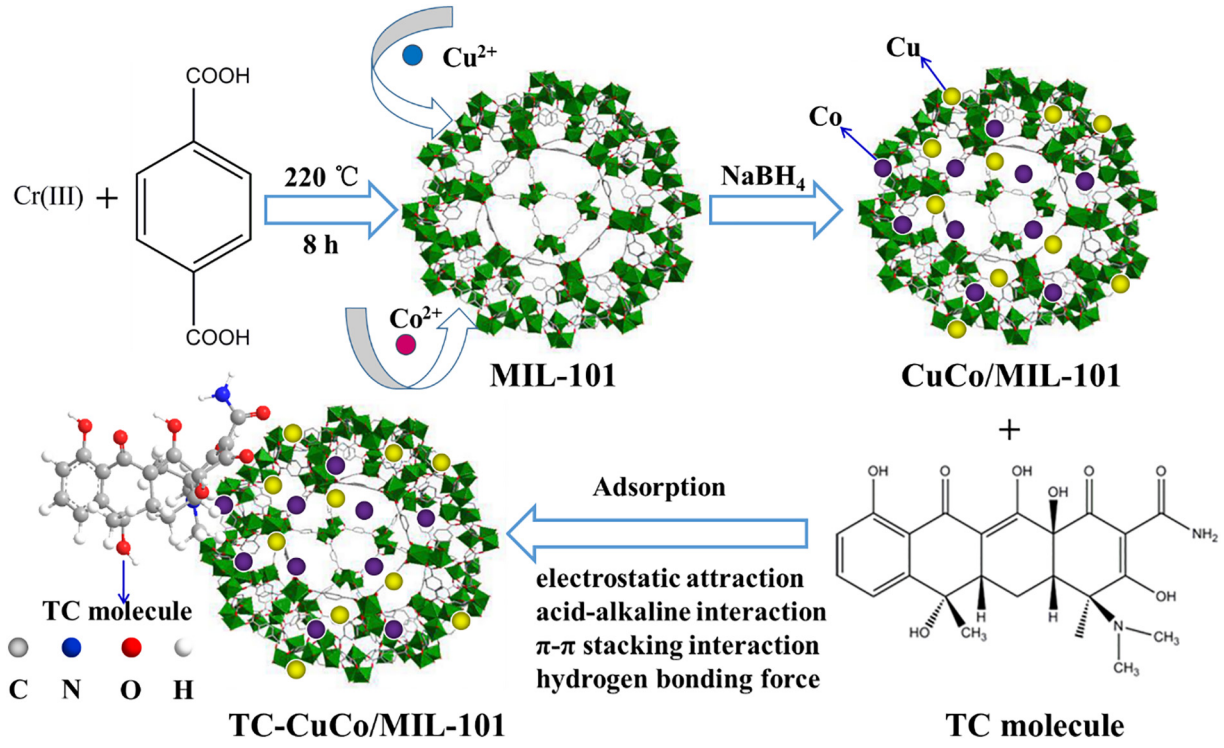

Scheme 1. Schematic diagrams of the synthesis of CuCo/MIL-101 and adsorption of tetracycline.

Fig. S6(b), it can be seen that the XRD pattern of adsorbent after two cycles showed no significantly change compared to fresh MLB-8. After four cycles, the intensity of the characteristic peaks was slightly reduced, but the positions of characteristic peaks did not change, demonstrating that the structure of MLB-8 still maintained intact. And the TEM image of MLB-8 after four cycles in Fig. S6(c) exhibited no change in morphology, which further confirmed that MLB-8 was reusable. Besides, the infrared spectrum of adsorbent in Fig. S6(d) was very similar to that of MLB-8 before reaction, which proved that the chemical stability of MLB-8 was better.

3.8. Adsorption mechanism

In general, adsorption of TC onto the MLB-8 is a complicated process that was jointly controlled by both physical and chemical interaction (shown in Scheme 1). Although the specific surface area was reduced to a certain extent compared with pure MIL-101 after loading CuCo BNPs, it was still larger than that of most conventional adsorbents. The strong physical adsorption was mainly ascribed to pore/size-selective adsorption, which facilitated the diffusion of TC molecules from the solutions to the outer surface of MLB-8 and into the pores and inner surface. In addition, the synergistic effect between Cu and Co binary components may be related to the strong chemical bonding force between transition metals and TC molecules, which greatly promoted the adsorption efficiency. Furthermore, the surface electronegativity of the composite material changed greatly after MIL-101 doping with CuCo BNPs, which would affect the electrostatic interactions between adsorbent and adsorbate. It turned out that electrostatic interactions made a great contribution to this adsorption process. Additionally, MIL-101 has Lewis acid properties, while the tertiary amine group of TC molecule is weakly alkaline due to the electronegativity of the nitrogen atom. The acid-alkaline interaction between the open metal sites and the tertiary amine groups was also one of the chemical adsorption mechanisms (Cirujano et al., 2012). Moreover, the aromatic structure of TC could interact with the benzene rings in the organic part of the MLB-8 through π-π interactions (Kim et al., 2013). Besides, hydrogen bonding forces may occur between functional groups in TC such as —OH, —NH_x as H-receptors and the O-containing groups including —COOH of MLB-8 (He et al., 2016). More detailed and accurate adsorption mechanisms should be further studied.

4. Conclusion

In this paper, the adsorption behavior and mechanism of TC onto CuCo/MIL-101 composite were investigated systematically. The adsorption capacity of MLB-8 with the best adsorption performance was 2.4 times higher than that of pure MIL-101. The measured pH_{ZPC} value of MLB-8 was 9.3. The adsorption performance was better under neutral to weak alkaline conditions, which may be attributed to the electrostatic interaction between positively charged MLB-8 and zwitterionic TC. The addition of Cl^- or SO_4^{2-} inhibited the adsorption of TC due to the competitive adsorption. However, the presence of humic acid in the solution enhanced TC adsorption. The kinetics and isotherm experimental data were best fitted by Elovich and Freundlich models, respectively. These results indicated that the adsorption of TC onto MLB-8 occurred predominantly chemical multi-layered adsorption showing a maximum adsorption capacity of 225.179 mg g^{-1}, which was higher than that of several adsorbents listed in literature. Meanwhile, the adsorption was spontaneous and endothermic, and the adsorption capacity enhanced with raising temperature. The obtained value of ΔH° was 29.851 kJ mol^{-1}, which suggested that the adsorption was a physicochemical adsorption process. In this study, the enhanced adsorption performance can be attributed to the pore/size-selective adsorption, chemical bonding, electrostatic interaction, acid-alkaline interaction, π-π stacking and hydrogen bonding forces. Furthermore, MLB-8 could be regenerated and reused by simple solvent washing and heat treatment under vacuum. The characterization results of XRD, FT-IR and TEM showed that MLB-8 had good chemical stability. All the results indicated that MLB-8 is a promising adsorbent for the TC removal from aqueous solutions.

Acknowledgements

This study was financially supported by the Key Research and Development Program of Hunan Province (2017SK2242), the National Natural Science Foundation of China (Grant Nos. 51578223, 51521006 and 51709103), the Natural Science Foundation of Hunan Province, China (Grant No. 2018JJ3242), China Postdoctoral Science Foundation (Grant No. 2018M630901), Hong Kong Scholars Program (XJ2018029).

Appendix A. Supplementary data

Supplementary data to this article can be found online at https://doi.org/10.1016/j.scitotenv.2018.08.434.

References

Barea, E., Montoro, C., Navarro, J.A.R., 2014. Toxic gas removal–metal–organic frameworks for the capture and degradation of toxic gases and vapours. Chem. Soc. Rev. 43, 5419–5430.
Chang, P.H., Li, Z., Jiang, W.T., Jean, J.S., 2009. Adsorption and intercalation of tetracycline by swelling clay minerals. Appl. Clay Sci. 46, 27–36.
Chen, Y.Z., Zhou, Y.X., Wang, H., Lu, J., Uchida, T., Xu, Q., Yu, S.H., Jiang, H.L., 2015. Multifunctional PdAg@MIL-101 for one-pot cascade reactions: combination of host–guest cooperation and bimetallic synergy in catalysis. ACS Catal. 5, 2062–2069.
Cirujano, F.G., Llabrés, F.X., Corma, A., 2012. MOFs as multifunctional catalysts: one-pot synthesis of menthol from citronellal over a bifunctional MIL-101 catalyst. Dalton Trans. 41, 4249–4254.
Dantas, G., Sommer, M.O.A., Oluwasegun, R.D., Church, G.M., 2008. Bacteria subsisting on antibiotics. Science 320, 100–103.
Deblonde, T., Cossu-Leguille, C., Hartemann, P., 2011. Emerging pollutants in wastewater: a review of the literature. Int. J. Hyg. Environ. Health 214, 442–448.
Duan, L., Li, L., Xu, Z., Chen, W., 2014. Adsorption of tetracycline to nano-NiO: the effect of co-existing Cu(ii) ions and environmental implications. Environ. Sci. Process Impacts 16, 1462–1468.
Férey, G., Mellot-Draznieks, C., Serre, C., Millange, F., Dutour, J., Surblé, S., Margiolaki, I., 2005. A chromium terephthalate-based solid with unusually large pore volumes and surface area. Science 309, 2040–2042.
Ferrando, R., Jellinek, J., Johnston, R.L., 2008. Nanoalloys: from theory to applications of alloy clusters and nanoparticles. Chem. Rev. 108, 845.
Gao, Y., Li, Y., Zhang, L., Huang, H., Hu, J., Shah, S.M., Su, X., 2012. Adsorption and removal of tetracycline antibiotics from aqueous solution by graphene oxide. J. Colloid Interface Sci. 368, 540–546.
Gu, B.H., Schmitt, J., Chen, Z.H., Liang, L.Y., McCarthy, J.F., 1994. Adsorption and desorption of natural organic matter on iron oxide: mechanisms and models. Environ. Sci. Technol. 28, 38–46.
Haque, E., Lee, J.E., Jang, I.T., Hwang, Y.K., Chang, J.S., Jegal, J., Jhung, S.H., 2010. Adsorptive removal of methyl orange from aqueous solution with metal-organic frameworks, porous chromium-benzenedicarboxylates. J. Hazard. Mater. 181, 535–542.
Hasan, Z., Jeon, J., Jhung, S.H., 2012. Adsorptive removal of naproxen and clofibric acid from water using metal-organic frameworks. J. Hazard. Mater. 209–210, 151–157.
He, J., Dai, J., Zhang, T., Sun, J., Xie, A., Tian, S., Yan, Y., Huo, P., 2016. Preparation of highly porous carbon from sustainable α-cellulose for superior removal performance of tetracycline and sulfamethazine from water. RSC Adv. 6, 28023–28033.
Hu, X.F., Lu, Y.K., Dai, F.N., Liu, C.G., Liu, Y.Q., 2013. Host-guest synthesis and encapsulation of phosphotungstic acid in MIL-101 via "bottle around ship": an effective catalyst for oxidative desulfurization. Microporous Mesoporous Mater. 170, 36–44.
Hu, T., Lv, H., Shan, S., Jia, Q., Su, H., Tian, N., He, S., 2016. Porous structured MIL-101 synthesized with different mineralizers for adsorptive removal of oxytetracycline from aqueous solution. RSC Adv. 6, 73741–73747.
Jiang, H.L., Xu, Q., 2011. Recent progress in synergistic catalysis over heterometallic nanoparticles. J. Mater. Chem. 21, 13705.
Jiang, J.Q., Yang, C.X., Yan, X.P., 2013. Zeolitic imidazolate framework-8 for fast adsorption and removal of benzotriazoles from aqueous solution. ACS Appl. Mater. Interfaces 5, 9837–9842.
Kara, M., Yuzer, H., Sabahb, E., Celik, M.S., 2003. Adsorption of cobalt from aqueous solutions onto sepiolite. Water Res. 37, 224–232.
Kemper, N., 2008. Veterinary antibiotics in the aquatic and terrestrial environment. Ecol. Indic. 8, 1–13.
Khan, N.A., Hasan, Z., Jhung, S.H., 2013. Adsorptive removal of hazardous materials using metal-organic frameworks (MOFs): a review. J. Hazard. Mater. 244–245, 444–456.
Kim, S.H., Shon, H.K., Ngo, H.H., 2010. Adsorption characteristics of antibiotics trimethoprim on powdered and granular activated carbon. J. Ind. Eng. Chem. 16, 344–349.
Kim, S.N., Kim, J., Kim, H.Y., Cho, H.Y., Ahn, W.S., 2013. Adsorption/catalytic properties of MIL-125 and NH_2-MIL-125. Catal. Today 204, 85–93.
Li, J., Zhu, Q.L., Xu, Q., 2015. Non-noble bimetallic CuCo nanoparticles encapsulated in the pores of metal–organic frameworks: synergetic catalysis in the hydrolysis of ammonia borane for hydrogen generation. Catal. Sci. Technol. 5, 525–530.
Li, H.Q., Hu, J.T., Meng, Y., Su, J.H., Wang, X.J., 2017. An investigation into the rapid removal of tetracycline using multilayered graphene-phase biochar derived from waste chicken feather. Sci. Total Environ. 603–604, 39–48.
Liu, Y., 2009. Is the free energy change of adsorption correctly calculated? J. Chem. Eng. Data 54, 1981–1985.
Liu, Y., Liu, Y.J., 2008. Biosorption isotherms, kinetics and thermodynamics. Sep. Purif. Technol. 61, 229–242.
Liu, Y., Xu, H., 2007. Equilibrium, thermodynamics and mechanisms of Ni^{2+} biosorption by aerobic granules. Biochem. Eng. J. 35, 174–182.
Maksimchuk, N., Timofeeva, M., Melgunov, M., Shmakov, A., Chesalov, Y., Dybtsev, D., Fedin, V., Kholdeeva, O., 2008. Heterogeneous selective oxidation catalysts based on coordination polymer MIL-101 and transition metal-substituted polyoxometalates. J. Catal. 257, 315–323.
Michael, I., Rizzo, L., McArdell, C.S., Manaia, C.M., Merlin, C., Schwartz, T., Dagot, C., Fatta-Kassinos, D., 2013. Urban wastewater treatment plants as hotspots for the release of antibiotics in the environment: a review. Water Res. 47, 957–995.
Milonjic, S.K., 2007. A consideration of the correct calculation of thermodynamic parameters of adsorption. J. Serb. Chem. Soc. 72, 1363–1367.
Milonjic, S.K., 2009. Comments on "Removal of uranium (VI) from aqueous solution by adsorption of hematite", by X. Shuibo, Z. Chun, Z. Xinghuo, Y. Jing, Z. Xiaojian, W. Jingsong. J. Environ. Radioact. 100, 921–922.
Ocampo-Pérez, R., Rivera-Utrilla, J., Gómez-Pacheco, C., Sánchez-Polo, M., López-Peñalver, J.J., 2012. Kinetic study of tetracycline adsorption on sludge-derived adsorbents in aqueous phase. Chem. Eng. J. 213, 88–96.
Oepen, B.V., Kördel, W., Klein, W., 1991. Sorption of nonpolar and polar compounds to soils: processes, measurements and experience with the applicability of the modified OECD-guideline 106. Chemosphere 22, 285–304.
Pezoti, O., Cazetta, A.L., Bedin, K.C., Souza, L.S., Martins, A.C., Silva, T.L., Júnior, O.O.S., Visentainer, J.V., Almeida, V.C., 2016. NaOH-activated carbon of high surface area produced from guava seeds as a high-efficiency adsorbent for amoxicillin removal: kinetic, isotherm and thermodynamic studies. Chem. Eng. J. 288, 778–788.
Pils, J.R.V., Laird, D.A., 2007. Sorption of tetracycline and chlortetracycline on K- and Ca-saturated soil clays, humic substances, and clay-humic complexes. Environ. Sci. Technol. 41, 1928–1933.
Priya, S.S., Radha, K.V., 2014. Equilibrium, isotherm, kinetic and thermodynamic adsorption studies of tetracycline hydrochloride onto commercial grade granular activated carbon. Int J Pharm Pharm Sci 7, 42–51.
Qi, B., Liu, Y., Zheng, T., Gao, Q., Yan, X., Jiao, Y., Yang, Y., 2018. Highly efficient capture of iodine by Cu/MIL-101. J. Solid State Chem. 258, 49–55.
Qiu, L.G., Xu, T., Li, Z.Q., Wang, W., Wu, Y., Jiang, X., Tian, X.Y., Zhang, L.D., 2008. Hierarchically micro- and mesoporous metal-organic frameworks with tunable porosity. Angew. Chem. Int. Ed. 47, 9487–9491.
Qu, X.P., Yu, Z.Q., Li, Z.P., Gui, X.Y., Jiang, R., Xu, Z.M., Chen, C.H., Peng, J., 2017. CoRh nanoparticles supported on ZIF-67 as highly efficient catalysts for hydrolytic dehydrogenation of ammonia boranes for chemical hydrogen storage. Int. J. Hydrog. Energy 42, 30037–30043.
Ronix, A., Pezoti, O., Souza, L.S., Souza, P.A.F., Bedin, K.C., Souza, P.S.C., Sliva, T.L., Melo, S.A.R., Cazetta, A.L., Almeida, V.C., 2017. Hydrothermal carbonization of coffee husk: optimization of experimental parameters and adsorption of methylene blue dye. J. Environ. Chem. Eng. 5, 4841–4849.
Rowsell, J.L.C., Yaghi, O.M., 2004. Metal–organic frameworks: a new class of porous materials. Microporous Mesoporous Mater. 73, 3–14.
Seo, P.W., Khan, N.A., Jhung, S.H., 2017. Removal of nitroimidazole antibiotics from water by adsorption over metal–organic frameworks modified with urea or melamine. Chem. Eng. J. 315, 92–100.
Song, P.P., Yang, Z.H., Zeng, G.M., Yang, X., Xu, H.Y., Wang, L., Xu, R., Xiong, W.P., Ahmad, K., 2017a. Electrocoagulation treatment of arsenic in wastewaters: a comprehensive review. Chem. Eng. J. 317, 707–725.
Song, Q., Fang, Y., Liu, Z., Li, L., Wang, Y., Liang, J., Huang, Y., Lin, J., Hu, L., Zhang, J., Tang, C., 2017b. The performance of porous hexagonal BN in high adsorption capacity towards antibiotics pollutants from aqueous solution. Chem. Eng. J. 325, 71–79.
Valcarcel, Y., Gonzalez Alonso, S., Rodriguez-Gil, J.L., Gil, A., Catala, M., 2011. Detection of pharmaceutically active compounds in the rivers and tap water of the Madrid Region (Spain) and potential ecotoxicological risk. Chemosphere 84, 1336–1348.
Wang, H., Yuan, X.Z., Wu, Y., Huang, H.J., Peng, X., Zeng, G.M., Zhong, H., Liang, J., Ren, M.M., 2013. Graphene-based materials: fabrication, characterization and application for the decontamination of wastewater and wastegas and hydrogen storage/generation. Adv. Colloid Interface Sci. 195–196, 19–40.
Wang, H., Yuan, X.Z., Wu, Y., Zeng, G.M., Dong, H.R., Chen, X., Dong, H.R., Chen, X.H., Leng, L.J., Wu, Z.B., Peng, L.J., 2016. In situ synthesis of In_2S_3@MIL-125(Ti) core–shell microparticle for the removal of tetracycline from wastewater by integrated adsorption and visible-light-driven photocatalysis. Appl. Catal. B Environ. 186, 19–29.
Wang, D.B., Jia, F.Y., Wang, H., Chen, F., Fang, Y., Dong, W.B., Zeng, G.M., Li, X.M., Yang, Q., Yuan, X.Z., 2018. Simultaneously efficient adsorption and photocatalytic degradation of tetracycline by Fe-based MOFs. J. Colloid Interface Sci. 519, 273–284.
Xie, A.T., Dai, J.D., He, J.S., Sun, J., Chang, Z.S., Li, C.X., Yan, Y.S., 2016. Converting obsolete copy paper to porous carbon materials with preeminent adsorption performance for tetracycline antibiotic. RSC Adv. 6, 13312–13322.
Xiong, W.P., Tong, J., Yang, Z.H., Zeng, G.M., Zhou, Y.Y., Wang, D.B., Song, P.P., R, Xu., Zhang, C., Cheng, M., 2017. Adsorption of phosphate from aqueous solution using iron-zirconium modified activated carbon nanofiber: performance and mechanism. J. Colloid Interface Sci. 493, 17–23.
Xiong, W.P., Zeng, G.M., Yang, Z.H., Zhou, Y.Y., Zhang, C., Cheng, M., Liu, Y., Hu, L., Wan, J., Zhou, C.Y., Xu, R., Li, X., 2018a. Adsorption of tetracycline antibiotics from aqueous solutions on nanocomposite multi-walled carbon nanotube functionalized MIL-53(Fe) as new adsorbent. Sci. Total Environ. 627, 235–244.
Xiong, W.P., Zeng, Z.T., Li, X., Zeng, G.M., Xiao, R., Yang, Z.H., Zhou, Y.Y., Zhang, C., Cheng, M., Hu, L., Zhou, C.Y., Qin, L., Xu, R., Zhang, Y.R., 2018b. Multi-walled carbon nanotube/amino-functionalized MIL-53(Fe) composites: remarkable adsorptive removal of

antibiotics from aqueous solutions. Chemosphere https://doi.org/10.1016/j.chemosphere.2018.07.084.
Xu, R., Yang, Z.H., Zheng, Y., Zhang, H.B., Liu, J.B., Xiong, W.P., Zhang, Y.R., Ahmad, K., 2017. Depth-resolved microbial community analyses in the anaerobic co-digester of dewatered sewage sludge with food waste. Bioresour. Technol. 244, 824–835.
Xu, R., Yang, Z.H., Wang, Q.P., Bai, Y., Liu, J.B., Zheng, Y., Zhang, Y.R., Xiong, W.P., Ahmad, K., Fan, C.Z., 2018. Rapid startup of thermophilic anaerobic digester to remove tetracycline and sulfonamides resistance genes from sewage sludge. Sci. Total Environ. 612, 788–798.
Yan, W.L., Bai, R., 2005. Adsorption of lead and humic acid on chitosan hydrogel beads. Water Res. 39, 688–698.
Yang, J.F., Ying, G.G., Zhao, J.L., Tao, R., Su, H.C., Chen, F., 2010. Simultaneous determination of four classes of antibiotics in sediments of the Pearl Rivers using RRLC-MS/MS. Sci. Total Environ. 408, 3424–3432.
Yang, W., Zheng, F., Lu, Y., Xue, X., Li, N., 2011. Adsorption interaction of tetracyclines with porous synthetic resins. Ind. Eng. Chem. Res. 50, 13892–13898.
Yang, Y., Hu, X., Zhao, Y., Cui, L., Huang, Z., Long, J., Xu, J., Deng, J., Wu, C., Liao, W., 2017. Decontamination of tetracycline by thiourea-dioxide-reduced magnetic graphene oxide: effects of pH, ionic strength, and humic acid concentration. J. Colloid Interface Sci. 495, 68–77.
Yu, F., Ma, J., Han, S., 2014. Adsorption of tetracycline from aqueous solutions onto multi-walled carbon nanotubes with different oxygen contents. Sci. Rep. 4, 5326.
Zhao, Y., Geng, J., Wang, X., Gu, X., Gao, S., 2011. Adsorption of tetracycline onto goethite in the presence of metal cations and humic substances. J. Colloid Interface Sci. 361, 247–251.
Zhao, Y., Gu, X., Gao, S., Geng, J., Wang, X., 2012. Adsorption of tetracycline (TC) onto montmorillonite: cations and humic acid effects. Geoderma 183–184, 12–18.
Zhou, L.J., Ying, G.G., Zhao, J.L., Yang, J.F., Wang, L., Yang, B., Liu, S., 2011. Trends in the occurrence of human and veterinary antibiotics in the sediments of the Yellow River, Hai River and Liao River in northern China. Environ. Pollut. 159, 1877–1885.
Zhou, Y.Y., Liu, X.C., Tang, L., Zhang, F.F., Zeng, G.M., Peng, X.Q., Luo, L., Deng, Y.C., Pang, Y., Zhang, J.C., 2017a. Insight into highly efficient co-removal of p-nitrophenol and lead by nitrogen-functionalized magnetic ordered mesoporous carbon: performance and modelling. J. Hazard. Mater. 333, 80–87.
Zhou, Y.Y., Liu, X.C., Xiang, Y.J., Wang, P., Zhang, J.C., Zhang, F.F., Wei, J.H., Luo, L., Lei, M., Tang, L., 2017b. Modification of biochar derived from sawdust and its application in removal of tetracycline and copper from aqueous solution: adsorption mechanism and modelling. Bioresour. Technol. 245, 266–273.
Zhou, C.Y., Lai, C., Xu, P., Zeng, G.M., Huang, D.L., Li, Z., Zhang, C., Cheng, M., Hu, L., Wan, J., Chen, F., Xiong, W.P., Deng, R., 2018. Rational design of carbon-doped carbon nitride/$Bi_{12}O_{17}Cl_2$ composites: a promising candidate photocatalyst for boosting visible-light-driven photocatalytic degradation of tetracycline. ACS Sustain. Chem. Eng. 6, 6941–6949.
Zhu, X., Li, B., Yang, J., Li, Y., Zhao, W., Shi, J., Gu, J., 2015. Effective adsorption and enhanced removal of organophosphorus pesticides from aqueous solution by Zr-based MOFs of UiO-67. ACS Appl. Mater. Interfaces 7, 223–231.